**12.9**     EXPERIMENTAL HIGH-RESOLUTION WSR-88D MEASUREMENTS
IN SEVERE STORMS

Rodger Brown[1], Bradley Flickinger[1,2], Eddie Forren[1,2], David Schultz[1,2],
Phillip Spencer[1,2], Vincent Wood[1], and Conrad Ziegler[1]

[1] NOAA, National Severe Storms Laboratory, Norman, OK
[2] Cooperative Institute for Mesoscale Meteorological Studies, University of Oklahoma, Norman, OK

## 1.    INTRODUCTION

Through use of Doppler velocity simulations, Wood et al. (2001) and Brown et al. (2002) have shown that stronger Doppler velocity signatures of mesocyclones and tornadoes, respectively,  can be obtained when WSR-88D (Weather Surveillance Radar–1988 Doppler) measurements are made at azimuthal sampling intervals of $0.5^o$ instead of the current intervals of $1.0^o$.  In addition, for signatures exceeding a particular Doppler velocity threshold, the signatures are detectable 50% farther in range using $0.5^o$ azimuthal sampling.

To help substantiate the simulation results, the National Severe Storms Laboratory's (NSSL) testbed WSR-88D radar (KOUN) collected high-resolution data in severe thunderstorms during Spring 2003.  The procedure was to record base data (reflectivity, mean Doppler velocity, spectrum width) at $0.5^o$ azimuthal resolution and at full range resolution of 0.25 km.  Then a recombination algorithm (e.g., Curtis et al. 2003) was used to produce the lower-resolution data ($1.0^o$, 1 km for reflectivity and $1.0^o$, 0.25 km for Doppler velocity and spectrum width) that are currently recorded and displayed by WSR-88Ds.

In this paper, we present comparisons of Doppler velocity signatures and reflectivity fields for high-resolution and current-resolution data fields.  The fields were displayed using NSSL's Warning Decision Support System II (WDSS II) display system.   Results show that high-resolution data produce mesocyclone signatures that typically are up to 15–20% stronger and reflectivity signatures that reveal otherwise poorly resolved or unresolved details.

## 2.    MESOCYCLONE SIMULATIONS

As an introduction to comparisons of high-

*Corresponding author address*: Dr. Rodger A. Brown, National Severe Storms Laboratory, 1313 Halley Circle, Norman, OK 73069;  e-mail  Rodger.Brown@noaa.gov

resolution to current-resolution measurements in mesocyclones, we present some of the simulation results of Wood et al. (2001).  A comparison of simulated Doppler radar scans across a mesocyclone for $1.0^o$ and $0.5^o$ azimuthal sampling is shown in Fig. 1.  The curves with dots along them represent the curves along which Doppler velocity measurements are made.  There are two factors illustrated in Fig. 1 that contribute to stronger  mesocyclone  signatures  with  $0.5^o$ azimuthal sampling.  First, the peaks of the measurement curve in Fig. 1b are closer to the pointed peaks of the "true" curve being sampled by the radar than in Fig. 1a.   The peaks are closer because the radar beam has to scan only half the distance in azimuth for $0.5^o$ sampling and therefore there is less smearing of the true curve. Second, with $0.5^o$ azimuthal sampling, there are twice as many data points along the measurement curve and therefore there is a greater probability that a data point will fall close to the peaks of the curve.   For the example in Fig. 1, the mean rotational velocity (average of the two extreme Doppler velocity values) is 16.2 m s$^{-1}$ for $1.0^o$ sampling, whereas the mean velocity is 19.0 m s$^{-1}$ for $0.5^o$ sampling—an increase of 17%.

The positions of data points along each measurement curve in Fig. 1 represent just one of many possible placements of data points along the curve.   Each possible placement would produce a different value for the mean rotational velocity.   In order to approximate all of these possibilities, Wood et al. (2001) divided the $1.0^o$ and  $0.5^o$  azimuthal intervals into 51 equally-spaced intervals for which mean rotational velocities were computed.   To produce realistic computations, random noise was added to individual data points before extreme values were selected for  the  mean  rotational  velocity computations.

It  was  important  to  add  random  noise because there is an inherent uncertainty in Doppler velocity measurements owing to a finite number of samples being used to compute mean Doppler velocity values.  In order to collect $0.5^o$ azimuthal data, it was assumed that the antenna

was rotating at the same speed as for $1.0^o$ data collection. With half the number of samples being collected for $0.5^o$ data, random noise increases by the square root of 2. Therefore, the standard deviation of random noise added to the simulated data point was increased by 1.414 (from 0.7 to 1.0 m s$^{-1}$) for $0.5^o$ data collection.

The resulting computations are presented in Fig. 2 as frequency distributions at three different ranges. The right (left) distribution in each panel is the distribution of mean rotational velocities computed from $0.5^o$ ($1.0^o$) data. It is curious that the $0.5^o$ distributions are narrower than the $1.0^o$ distributions at all ranges. With appreciably more random noise being added to the $0.5^o$ data points, one would expect the $0.5^o$ distributions to be significantly broader. Evidently, the reduced smearing and more closely spaced mean Doppler velocity values associated with $0.5^o$ sampling more than offset effects of greater random noise.

It is obvious in Fig. 2 that, on average, data collected at $0.5^o$ azimuthal intervals produce stronger mean rotational velocities for mesocyclones. There is a slight overlap of the two distributions, indicating that on rare occasions the $1.0^o$ data will produce stronger rotational velocities.

## 3. MESOCYCLONE COMPARISONS

During Spring 2003, KOUN collected high-resolution data ($0.5^o$, 0.25 km) in Oklahoma mesocyclones on six days during April and May. These data were then recombined into current WSR-88D resolution data ($1.0^o$, 0.25/1.0 km) using the Curtis et al. (2003) approach. Doppler velocity displays of these data sets were visually inspected for mesocyclone signatures and signature characteristics were tabulated. About 600 pairs of high- and current-resolution signatures were found at various elevation angles on those six days.

Plotted in Fig. 3 are ratios of mean rotation velocity from the $0.5^o$ data to mean velocity from the $1.0^o$ data. As expected based on Fig. 2, the vast majority of $0.5^o$ mesocyclone signatures were stronger than $1.0^o$ signatures, with most being up to 15-20% stronger. As also expected, some (about 10%) of the $1.0^o$ signatures were stronger.

The data in Fig. 3, reinforced by the simulation results in Fig. 2, indicate that higher-resolution $0.5^o$ data collection would benefit the issuing of severe storm warnings. On average, mesocyclone signatures are stronger with $0.5^o$ data collection. Being stronger, they exceed a given threshold value earlier in their lifetime and,

as indicated by the Wood et al. (2001) simulations, they continue to exceed the threshold up to 50% farther in range.

## 4. REFLECTIVITY COMPARISONS

Reflectivity signatures in severe storms are more difficult to quantify than Doppler velocity signatures, so advantages of $0.5^o$/0.25 km data collection over $1.0^o$/1.0 km data collection are illustrated by comparing images on reflectivity displays. Since high-resolution reflectivity data have eight times the resolution of current WSR-88D reflectivity data, dramatic improvements can be anticipated.

### a. Surface boundaries

Figure 4 shows a cold front that has passed southeastward over KOUN and a ridge to the southwest of the radar. As the front moved over the ridge, a wave developed on it and a hailstorm formed at the occluded apex. The high-resolution image on the right shows more continuity in the enhanced radar return along the cold front, especially in the vicinity of the growing storm.

During the next 70 min, the storm split into a left-moving storm and a right-moving storm. The gust front associated with the right-moving storm is shown in Fig. 5. While the current-resolution display contains the suggestion of a possible gust front, the high-resolution display shows it very clearly. The high-resolution gust front position is confirmed by high-resolution Doppler velocity convergence. Generally, boundaries indicated by high-resolution data (both reflectivity and Doppler velocity) have greater temporal continuity than provided by current-resolution data. This suggests that the combination of high-resolution reflectivity and Doppler velocity data can be used to improve automated boundary detection algorithms.

### b. Bounded weak echo regions

A bounded weak echo region (BWER) is a midaltitude reflectivity minimum that indicates the presence of a strong updraft within a severe thunderstorm. The BWER is caused by new hydrometeors that are carried rapidly aloft by the updraft and do not have time to grow to radar-detectable sizes until they are in the upper portions of the storm (e.g., Glickman 2000).

Figures 6–10 show BWERs in different storms at progressively farther ranges (45 to 195 km) from KOUN. The current-resolution display in

Fig. 6 does not obviously indicate the presence of the BWER that is readily evident in the southwest portion of the storm in the high-resolution display. The storm at 80-km range in Fig. 7 reveals the presence of a BWER at both resolutions, but the minimum is more pronounced in the high-resolution display. Beyond 100 km from the radar, the BWER is only detected in the high-resolution display (Figs. 8–10).

Reflectivity color scales along the right side of the displays are incremented by 5 dBZ starting with 20 dBZ (second green color). The high-resolution BWERs are so obvious because the minimum reflectivity values are one to two color categories (5-10 dBZ) lower than with the current resolution.

*c. Hook echoes*

Figure 11 shows an echo at 140-km range that is rather nondescript on the current WSR-88D display. However, high-resolution data reveal the presence of a hook echo on the storm's right rear flank. Doppler velocity measurements indicate the presence of a mesocyclone signature associated with the hook. The storm produced an F0 tornado.

A dramatic hook echo at 40-km range is shown in Fig. 12. Radar detection of debris rotating around an F3 tornado produced the "ball" at the end of the hook echo [see Schuur et al. (2004) for discussion of polarization detection of debris]. Although the current radar display adequately portrays the presence of the hook, the high-resolution display reveals greater detail.

## 5. CONCLUDING COMMENTS

We compared displays of current WSR-88D Doppler velocity and reflectivity signatures in severe storms with displays showing higher-resolution signatures. High-resolution displays have twice the number of Doppler velocity and spectrum width data points and eight times the number of reflectivity data points.

At all ranges, high-resolution data did a much better job in depicting severe storm character-istics. Mean rotational velocities for meso-cyclones based on high-resolution mesocyclone signatures were up to 15–20% stronger on average than velocities based on current-resolution signatures. At ranges greater than 100 km, the high-resolution displays revealed severe storm signatures, such as bounded weak echo regions and hook echoes, that were not apparent on the current-resolution displays.

These findings hold great promise for helping to improve severe storm warning capabilities for National Weather Service forecast offices. It appears that high-resolution data may be available in a couple of years. Initially, high-resolution data probably would be used only for the displays, with current-resolution data being used for the various meteorological algorithms.

Several things must occur before high-resolution displays can become operational. In order to have available both current-resolution and high-resolution data, the recombination algorithm used in this study will have to be thoroughly tested and evaluated. It will not be possible to collect high-resolution data until after Open Radar Data Acquisition (ORDA) Units are installed at radar sites. With higher data transmission rates between the ORDA and Open Radar Product Generator (ORPG), data compression techniques will have to be employed.

## 6. REFERENCES

Brown, R. A., V. T. Wood, and D. Sirmans, 2002: Improved tornado detection using simulated and actual WSR-88D data with enhanced resolution. *J. Atmos. Tech.*, **19**, 1759–1771.

Curtis, C. D., S. M. Torres, and E. Forren, 2003: High-resolution WSR-88D base data on the KOUN research radar. *Preprints*, 31st Conf. on Radar Meteor., Seattle, Amer. Meteor. Soc., 964–966.

Glickman, T. S., (ed.) 2000: *Glossary of Meteorology*, 2nd edition, Amer. Meteor. Soc., 855 pp.

Schuur, T. J., A. V. Ryzhkov, P. L. Heinselman, D. W. Burgess, and K. A. Scharfenberg, 2004: The Joint Polarization Experiment – A summary of dual-polarization WSR-88D radar data collection and analysis. *Preprint CD*, 20th Conf. on Interactive Information Processing Systems, Seattle, Amer. Meteor. Soc., Paper 12.1.

Wood, V. T., R. A. Brown, and D. Sirmans, 2001: Technique for improving detection of WSR-88D mesocyclone signatures by increasing angular sampling. *Wea. Forecasting*, **16**, 177–184.
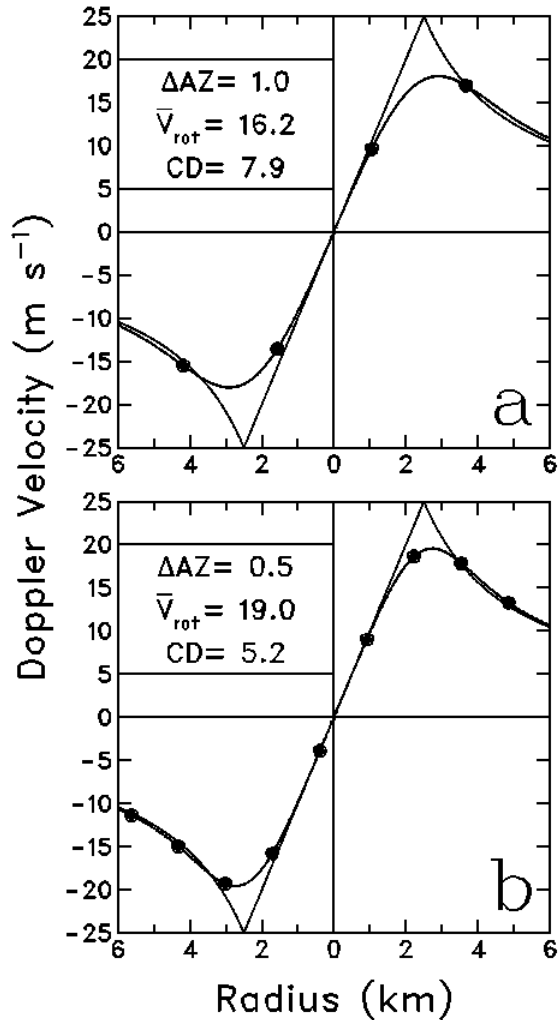
**Fig. 1.** Relationship of data points relative to the azimuthal profile of a mesocyclone signature for azimuthal sampling intervals (ΔAZ) of (a) 1.0° and (b) 0.5°. The measurement curve with rounded peaks (along which data points fall) represents the Doppler velocity azimuthal profile of the mesocyclone signature if the radar were able to make measurements in a continuous manner across the mesocyclone at 150 km range. Data points (black dots) represent locations of successive Doppler velocity measurements collected at ΔAZ intervals as the radar beam scans across the mesocyclone. The model ("true") azimuthal profile is indicated by the curve with pointed peaks corresponding to a typical mesocyclone having a peak rotational velocity of 25 m s$^{-1}$ at a core diameter of 5 km. Deduced values of mean rotational velocity ($\overline{V_{rot}}$) in m s$^{-1}$ and core diameter (CD) in km are indicated. From Wood et al. (2001).
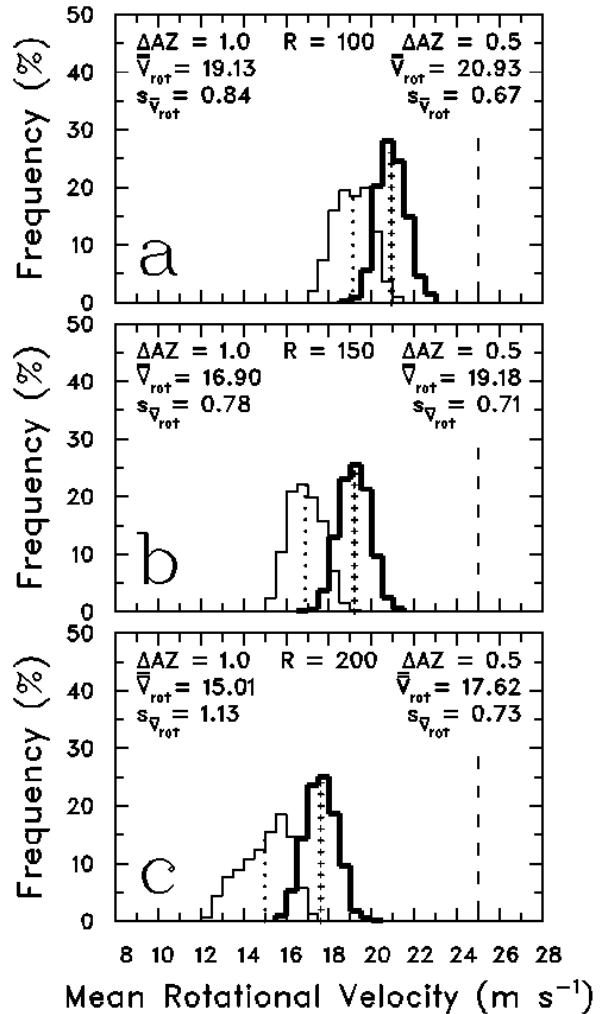
**Fig. 2.** Frequency distributions of mesocyclone mean rotational velocity estimates arising from the chance placement of radar beams relative to the peaks of the measurement curves (as in Fig. 1) at ranges of (a) 100 km, (b) 150 km, and (c) 200 km. Thin (thick) lines correspond to 1.0° (0.5°) azimuthal data collection. The averages of the mean rotational velocity values ($\overline{\overline{V_{rot}}}$) are indicated by vertical lines with plus signs. The vertical dashed line represents the peak rotational velocity of the model mesocyclone. The standard deviation of the mean rotational velocity values is given by $s_{\overline{\overline{V_{rot}}}}$ (m s$^{-1}$). From Wood et al. (2001).
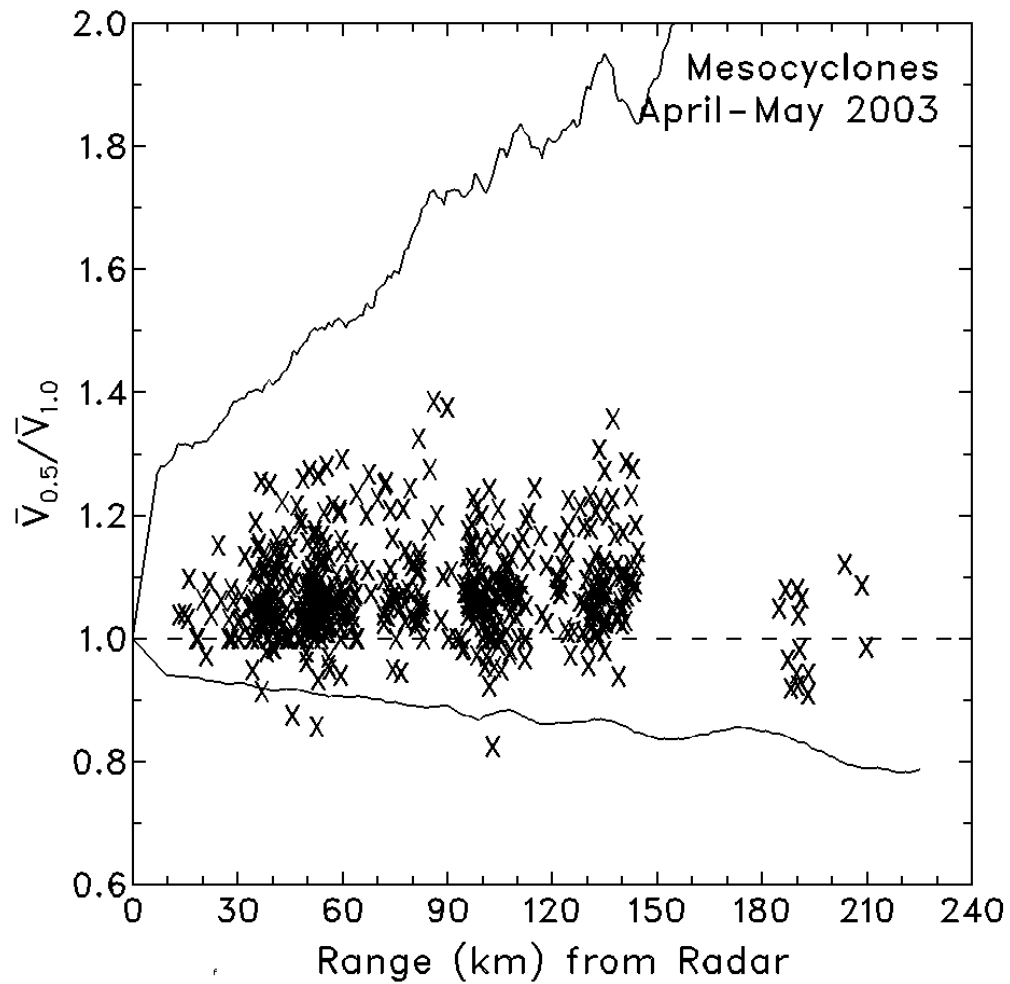
**Fig. 3.** Ratios of mean rotational velocity from 0.5° azimuthal data collection to mean rotational velocity from 1.0° azimuthal data collection plotted as a function of range from the radar. Horizontal dashed line indicates no improvement using 0.5° azimuthal sampling. Upper and lower curves represent likely extreme ratios based on the simulations of Wood et al. (2001).
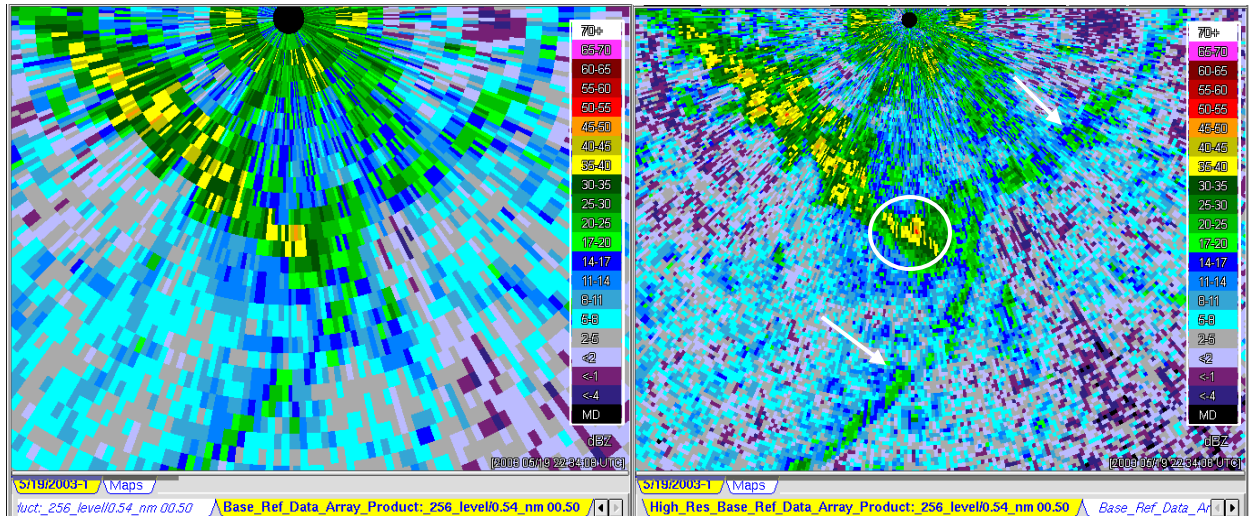
**Fig. 4.** Current-resolution (left) and high-resolution (right) reflectivity displays of a cold frontal boundary (white arrows) extending basically from southwest to northeast across the display (0.5° elevation angle). The strong echo (white circle) 13 km due south of the radar (black dot at top) is the beginning of a hailstorm that formed along the cold front as it moved southeastward over the northwest-southeast oriented ridge (line of yellow and orange echoes).
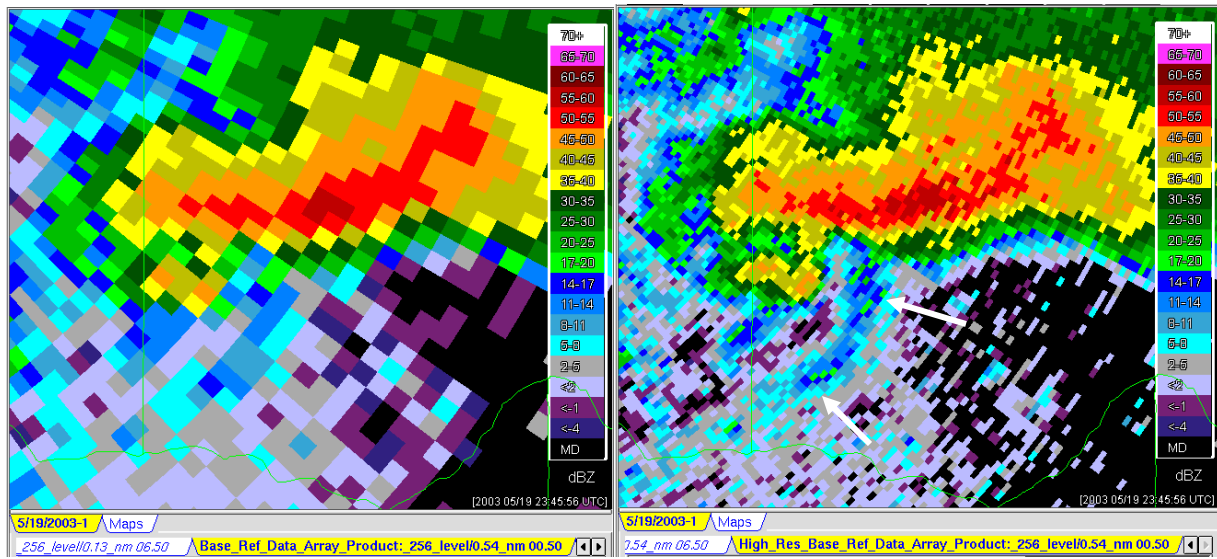


**Fig. 5.** Current-resolution (left) and high-resolution (right) reflectivity displays of a hailstorm at a height of 0.5 km (0.5° elevation angle). The white arrows indicate the location of the gust front about 40 km from the radar.
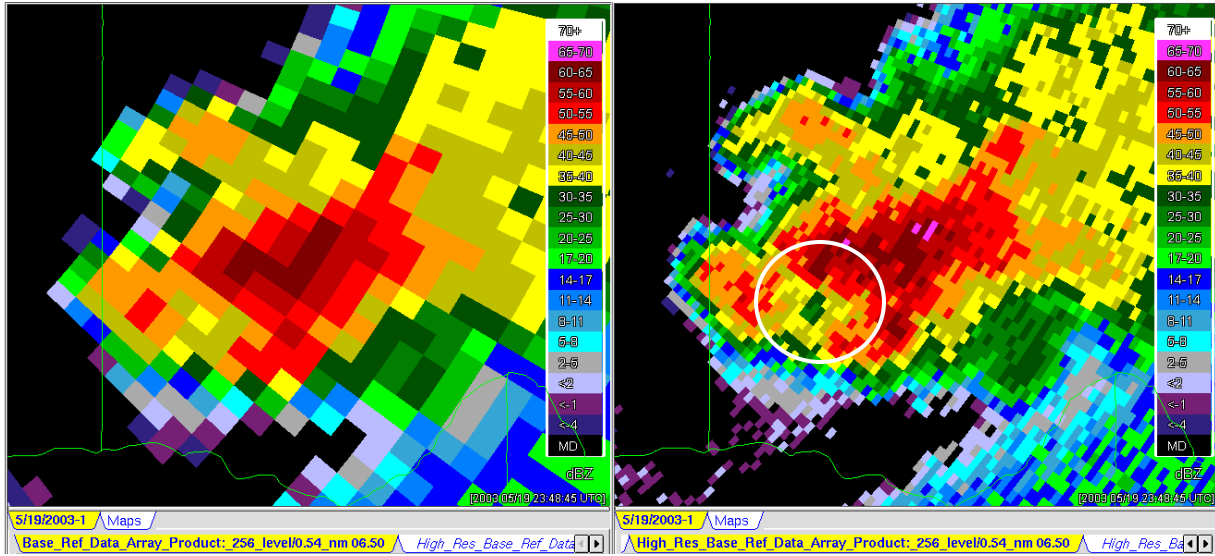
**Fig. 6.** Current-resolution (left) and high-resolution (right) reflectivity displays (6.5° elevation) of a severe storm containing a bounded weak echo region (inside white circle). The BWER is at a range of 45 km and height above radar of 5.2 km.
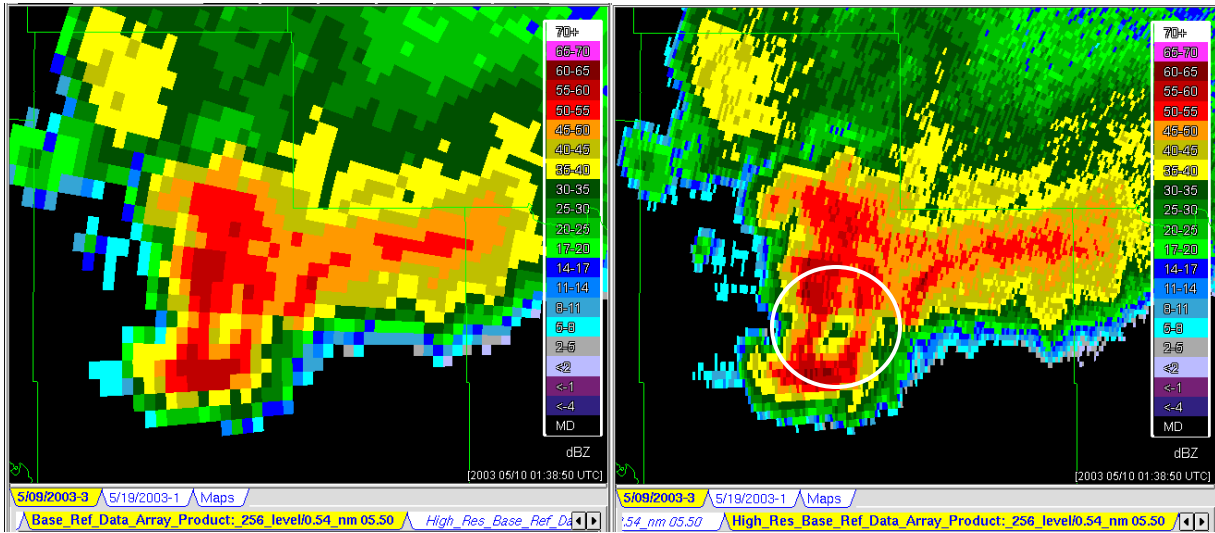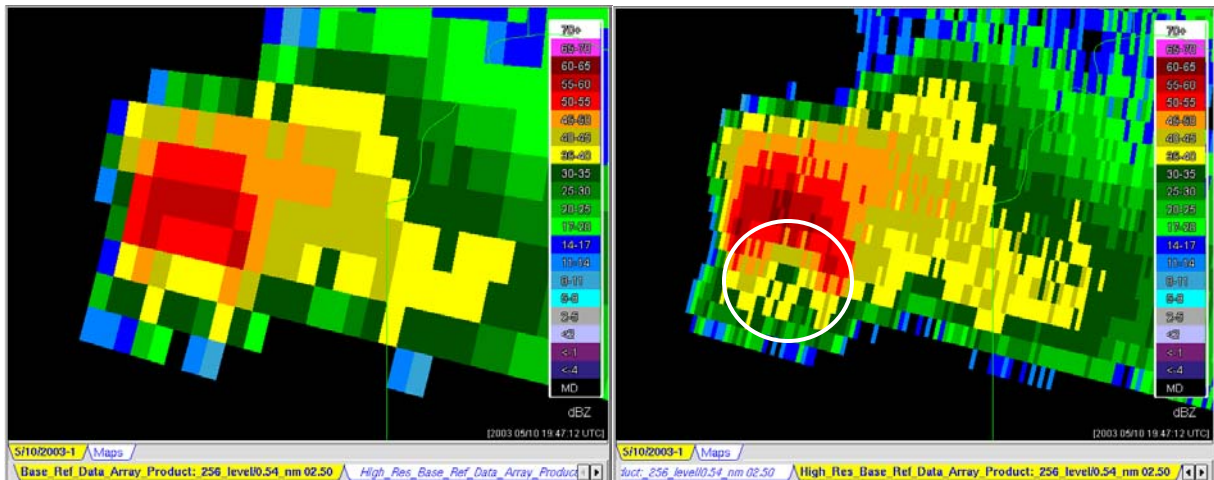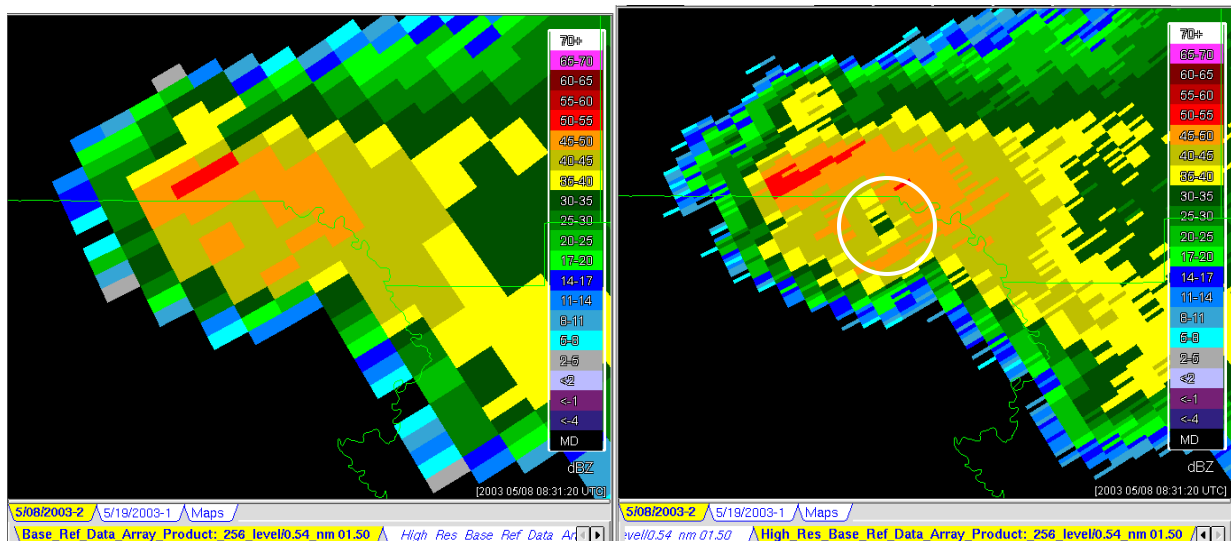


**Fig. 7.** Current-resolution (left) and high-resolution (right) reflectivity displays (5.5° elevation) of a severe storm containing a bounded weak echo region (inside white circle). The BWER is at a range of 80 km and height above radar of 8.3 km.

**Fig. 8.** Current-resolution (left) and high-resolution (right) reflectivity displays (2.5$^o$ elevation) of a severe storm containing a bounded weak echo region (inside white circle). The BWER is at a range of 115 km and height above radar of 5.8 km.
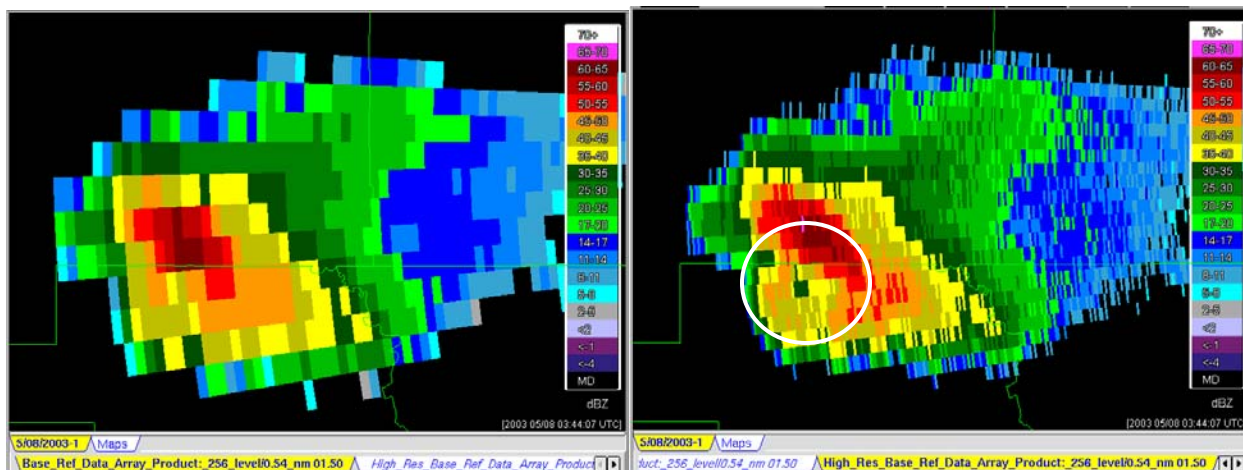


**Fig. 9.** Current-resolution (left) and high-resolution (right) reflectivity displays (1.5$^o$ elevation) of a severe storm containing a bounded weak echo region (inside white circle). The BWER is at a range of 140 km and height above radar of 4.9 km.

**Fig. 10.** Current-resolution (left) and high-resolution (right) reflectivity displays (1.5$^\circ$ elevation) of a severe storm containing a bounded weak echo region (inside white circle). The BWER is at a range of 195 km and height above radar of 7.1 km.
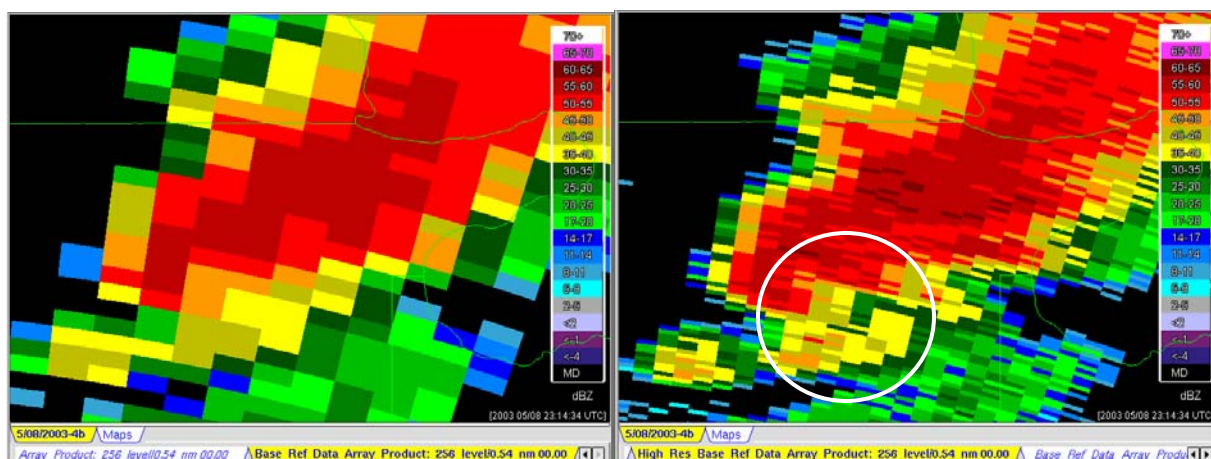


**Fig. 11.** Current-resolution (left) and high-resolution (right) reflectivity displays (0.0$^\circ$ elevation) of a hook echo (inside white circle) at a range of 140 km and height above radar of 1.6 km.
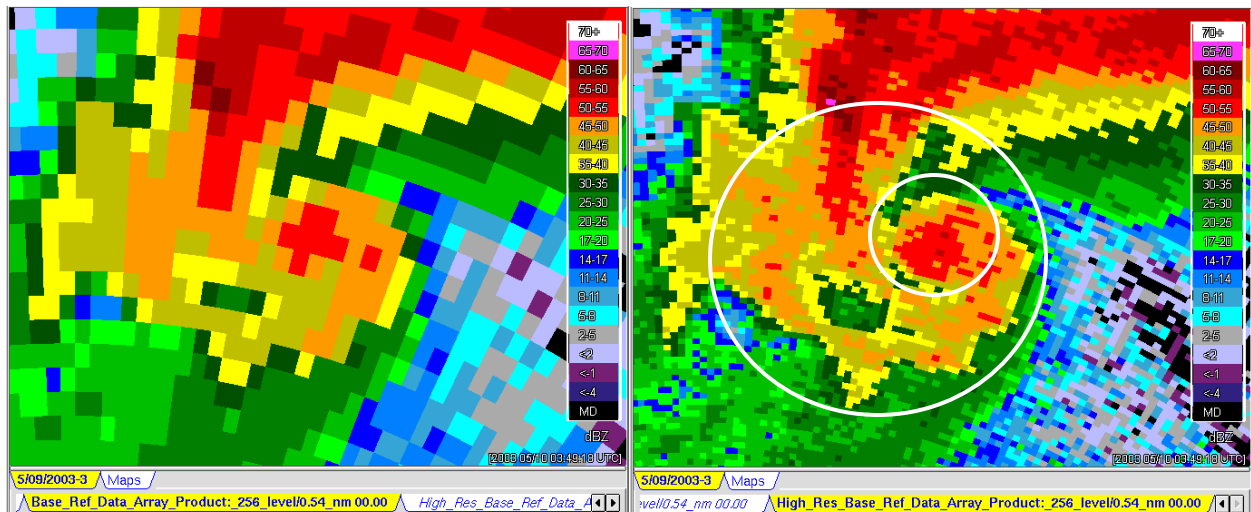
**Fig. 12.** Current-resolution (left) and high-resolution (right) reflectivity displays (0.0° elevation) of a debris echo (inside smaller white circle) associated with an F3 tornado at the end of a hook echo (inside larger white circle) at a range of 40 km and height above radar of 0.12 km.